Environmental Science Nano

ROYAL SOCIETY OF CHEMISTRY

PAPER

View Article Online
View Journal | View Issue

Cite this: *Environ. Sci.: Nano*, 2022, **9**, 4150

Lipidomic analysis probes lipid coronas on hydrophilic nanoparticles from natural lung surfactant†

Xuan Bai, ‡[a] Sin Man Lam,‡[bc] Pengcheng Nie,[de] Ming Xu, [ef] Sijin Liu, [ef] Guanghou Shui*[be] and Guoqing Hu *[a]

The large respiratory surface and high permeability make the lung promising in drug delivery of inhaled nanoparticles (NPs) as a portal and susceptible to nanosized airborne pollutions. Inhaled NPs first interact with the lung surfactant (LS) after depositing in the lung, where NPs tend to adsorb the LS molecules to form a biomolecular corona on their surface. Despite the extensive studies of protein coronas from blood plasma or serum, lipid coronas that are constituted by LS molecules are rarely investigated. Herein, we combine high-performance liquid chromatography-mass spectrometry and molecular dynamics simulation to unravel how a lipid corona is formed on hydrophilic NPs from a natural LS. Experiments demonstrate that positive surface charge, long incubation time, and external sonication can promote the formation of a complete lipid corona with compositions different from the bulk LS. Complementary to the experiments, molecular simulations indicate that the surface charge of NPs plays a vital role in the interactions of NPs with both zwitterionic and anionic lipids, which determines the wrap of the LS bilayer on the NP. In addition, the difference in the lipid composition between the corona and the bulk LS is caused by the affinity of NPs with lipids and the intrinsic structure of lipids. These results suggest that it is possible to control the formation and composition of lipid coronas on hydrophilic NPs by tuning the surface coating of NPs and incubation conditions.

Received 8th July 2022,
Accepted 21st September 2022

DOI: 10.1039/d2en00653g

rsc.li/es-nano

Environmental significance

Inhaled nanoparticles (NPs) can reach the deep lung where they interact with lung surfactant (LS). Formation of the lipid corona *via* adsorption of natural LS is crucial in assessing the biological effect and toxicity of inhaled NPs. Using high-performance liquid chromatography-mass spectrometry, we demonstrate a weak adsorption of the LS lipids on the negatively charged NPs and a complete formation of the bilayer corona on the positively charged NPs upon sonication or long-time incubation, where the lipid compositions of the corona differ from the pristine LS. The present results suggest that it is feasible to avoid or promote the formation of the lipid corona by controlling the surface charge of NPs for the safe use of NPs in biotechnology and nanomedicine.

Nanoparticles (NPs) play an essential role in fostering a wide range of applications including pharmaceuticals,[1] imaging,[2] and diagnosis.[3] Either on purpose or not, NPs immersed in biological fluids often acquire a selective layer of

[a] *Department of Engineering Mechanics, State Key Laboratory of Fluid Power and Mechatronic Systems, Zhejiang University, Hangzhou, China. E-mail: ghu@zju.edu.cn*
[b] *State Key Laboratory of Molecular Developmental Biology, Institute of Genetics and Developmental Biology, Chinese Academy of Sciences, Beijing, China. E-mail: ghshui@genetics.ac.cn*
[c] *LipidALL Technologies Company Limited, Changzhou, China*
[d] *State Key Laboratory of Nonlinear Mechanics, Institute of Mechanics, Chinese Academy of Sciences, Beijing, China*
[e] *University of the Chinese Academy of Sciences, Beijing, China*
[f] *State Key Laboratory of Environmental Chemistry and Ecotoxicology, Research Center for Eco-Environmental Sciences, Beijing, China*

† Electronic supplementary information (ESI) available: Characterization of NPs and Curosurf®, detailed composition of the LS lipids used in CGMD simulations (Tables S1–S4); TEM images for NPs, relative lipid distribution in the corona on neutral NPs, absolute lipid distribution in the corona on positively charged NPs, proportion of saturated and unsaturated lipids in bulk LS, snapshots for the simulations of the interactions between NPs and dispersed LS, interaction energy per molecule of NPs with different lipid species, time evolution of the interaction energy of the NPs with the LS bilayer (Fig. S1–S7); calculation of the amount and density of the lipid coronas (Note S1) (PDF). List of all lipids determined in the bulk LS and corona of NPs (XLSX). Script for assigning surface charge of CG silica NP and Gromacs input file for running MD simulations (RAR). See DOI: https://doi.org/10.1039/d2en00653g
‡ These authors contributed equally.

biomolecules, giving rise to a biomolecular corona that confers a new identity for NPs and affects the eventual fate of NPs.[4,5] So far, protein coronas from blood plasma or serum have been the subject of much systematic investigation.[6–10] Formed within seconds or minutes upon exposure to human plasma, the amount and composition of the protein corona depend on the properties of pristine NPs and also change over incubation time.

Depending on the way to enter the human body, NPs will encounter very different environments. Among various biological fluids that interact with NPs, lung surfactant (LS) is rarely studied but no less important. LS is a lipid–protein complex of approximately 90% lipids, most of which are phospholipids, cholesterol, and 10% surfactant proteins such as SP-A, SP-B, SP-C and SP-D by weight.[11] Lining on the alveoli surface, LS is responsible for reducing the surface tension of alveoli while acting as the first-line barrier against the inhaled NPs or pathogens.[12–15] Only a few studies have focused on the development of lipid coronas that are constituted by the LS components on the inhaled NPs.[16–19] Different from the common protein corona, phospholipids, the major component in lipid coronas, largely determine the biological recognition of the NPs.[20–24] For example, phosphatidylinositol (PI) specially binds to SP-D that is responsible for innate immune response,[25] and anionic phosphatidylglycerol (PG) and phosphatidylserine (PS) in the lipid corona notably strengthen the macrophage internalization of NPs compared to zwitterionic phospholipids.[23,26] Therefore, in order to assess the biological effects of the inhaled NPs properly, it is crucial to understand the formation of the lipid corona and determine its compositions as well.

Despite the importance of the lipid corona in inhalation scenarios, the understanding of the lipid corona is still very limited and needs to be advanced. Phospholipids, owing to their amphipathicity, tend to form well-constructed vesicular structures in the lung fluids, and thus may go through an adsorption process different from that suggested by existing models for individual molecules.[27,28] Although bronchoalveolar lavage fluid (BALF) is an ideal model to mimic the real fluid environment that NPs encounter in the lung,[17,29,30] it contains not only surfactant proteins but also various other types of proteins that may participate in and distort the interactions of NPs with LS lipids. Exogenous lung surfactant, such as Curosurf®, preserves the diversity and complexity of the lipid compositions in natural LS but with only 1% hydrophobic surfactant proteins in wt%.[31] Thus, it becomes a widely used model to investigate how the interactions of NPs with LS, especially lipids in LS, affect the formation of lipid coronas.[18,29,32–34] However, these studies rely on qualitative measurements that lack quantitative understanding of to what extent a complete lipid corona can be formed on NPs and which lipids are preferred to be adsorbed on NPs. Further molecular details on the interactions between NPs and LS lipids are also needed for establishing a comprehensive correlation between the properties of NPs and formation of lipid coronas.

Before the term 'lipid corona' was introduced to the nanoscience community, there has been extensive research on lipid adsorption on NPs in the interest of the supported lipid bilayer and engineered lipid-coated NPs.[35–38] The transformation of liposome to a supported bilayer on a hydrophilic surface is balanced by the deformation of liposome and the attraction interactions (*e.g.*, van der Waals and electrostatic forces) between the liposome and the surface,[39,40] which can be controlled by the lipid composition, surface properties and environmental conditions.[41–45] When the surface becomes hydrophobic, adsorption of liposomes is driven by hydrophobic interactions, leading to the formation of a supported monolayer.[46,47] Considering that LS is mainly composed of lipids, LS lipids might have similar adsorption phenomena to the liposome. However, due to the complexity of the lipid composition of natural LS, it would be harder to clarify the mechanism of LS lipid adsorption on the NP surface compared to model liposomes.

Herein, we combined high-performance liquid chromatography-mass spectrometry (HPLC-MS) and molecular dynamics (MD) simulations to study the development of the lipid corona on silica NPs with different charges upon contact with a natural LS. LC-MS lipidomic analysis was used to assess whether a complete lipid corona was formed under different incubation conditions and whether the compositions of the lipid corona differed from the bulk LS by quantitatively probing the adsorbed lipids on NPs. MD simulations were used to reveal the molecular structure and interaction between NP and LS, helping to understand how charge influences the adsorption of LS lipids on NPs.

Experimental

Characterization of the silica NPs and LS

Bare silica NPs and neutral aminated silica NPs were purchased from Nanjing Nanorainbow Biotechnology Co., Ltd (Nanjing, China), and positively charged aminated silica NPs were purchased from Creative Diagnostics (New York, USA). Curosurf® (Chiesi Pharmaceuticals, Parma, Italy), a porcine minced lung surfactant extract, was used as the LS model that comprises 99% phospholipids and 1% surfactant proteins.[31] The hydrodynamic diameter and zeta potential of NPs and Curosurf® were obtained using a Zetasizer Nano ZSP (Malvern Instruments, USA). The geometric size and shape of NPs were observed by transmission electron microscopy (TEM, Hitachi HT7700, Japan).

Incubation and separation of NPs with the LS

Silica NPs and Curosurf® were diluted in MilliQ-water to 1 mg ml^{-1} and 0.8 mg ml^{-1} respectively, and then mixed with equal volumes for incubation referred to previous protocols.[18] At the condition of 1-hour and 24-hour incubation, the Curosurf® solution was sonicated briefly by bath sonication (KQ5200DE, 55 kW, Kunshan, China) before

incubation with NPs for decreasing the aggregation of Curosurf® and the mixed solution was incubated at 37 °C without active mixing. At the condition of 1-hour incubation with sonication, NPs and Curosurf® were incubated at 37 °C for 40 minutes, and then sonicated by bath sonication for 20 minutes which was regarded as reaching equilibrium for mixing the NPs and LS.[18] The NP–LS complex was centrifuged through a sucrose cushion (50%) for 5 min at 13 000 rpm, followed by redispersion with phosphate buffered saline into a new tube and direct centrifugation for 5 min at 13 000 rpm. The supernatant was discarded and the NP–LS pellets were frozen at −80 °C until further analysis.

Lipid extraction and LC-MS measurement of the adsorbed LS

LS lipids were extracted using a modified Bligh and Dyer's extraction procedure (double rounds of extraction) and dried in the SpeedVac under OH mode. Prior to analysis, lipid extracts were resuspended in chloroform : methanol 1 : 1 (v/v) spiked with appropriate internal standards. Note that the recovery methods of the lipids on NPs could be also optimized using Zhang's and Lee's protocols.[48,49] All lipidomic analyses were carried out on an Agilent 1260-HPLC system coupled with a QTRAP 5500 PLUS system (Sciex) as described previously.[50] Lipids were analyzed under electrospray ionization mode by targeted multiple-reaction monitoring (MRM) on a QTRAP 5500. Source parameters were as follows, CUR 12, TEM 400 °C, GS 1 = 20, GS 2 = 20. PC, SM and LPC were analyzed in the positive ion mode and identified based on their characteristic head group product ion fragment at m/z 184.1. The remaining phospholipids including PE, PI, PG and PA (and their corresponding lysophospholipids) were identified based on characteristic product ions at m/z 140.1, 241.1, 153.0 and 153.0, respectively. Individual lipid classes were cleanly separated under the gradient programme adopted, which utilized a Phenomenex Luna Silica 3 μm column (i.d. 150 × 2.0 mm) with mobile phase A (chloroform : methanol : ammonium hydroxide, 89.5 : 10 : 0.5) and mobile phase B (chloroform : methanol : ammonium hydroxide : water, 55 : 39 : 0.5 : 5.5) at a flow rate of 270 μL min^{-1} and column oven temperature at 25 °C. The gradient programme initiated with 2% B that was maintained for the first two min, which was increased to 40% B over the next one min, and was maintained at 40% B for another five min. At the 8th min, % B was increased to 100% over 0.1 min and maintained at 100% B until the 16th min. The gradient was then re-equilibrated back to 2% B for 4 min before the next injection was made. All quantification experiments were conducted using internal standard calibration. Individual polar lipid species were quantified by referencing to spiked internal standards of the same lipid class, including PC-14:0/14:0, PE14:0/14:0, PS-d31, PA-17:0/17:0, PG-14:0/14:0, SM-d18:1/12:0, LPC-17:0, LPE-17:0, LPI-17:1, LPA-17:0, LPS-17:1 obtained from Avanti Polar Lipids (Alabaster, AL, USA) and PI-8:0/8:0 from Echelon Biosciences (Salt Lake City, UT, USA). Quantitated levels of individual lipids in μmol were calculated according to the equation:

$$\text{Level of lipids X (μmol)} = \frac{\text{peak area of lipid X}}{\text{peak area of internal standard}} \times \text{concentration of internal standard} \times \text{sample volume}$$

Force field and set up for molecular simulations

We studied the interaction between the silica NPs with different surface charges and LS using CGMD simulations with the Martini force field.[51] In CG MD simulations, a cluster of atoms is considered as one bead, which decreases the total freedom of the atoms to increase the spatial and temporal scales of the simulation.[52] The BMW (big multipole water) model was adopted to replace the original Martini water model, which performed better in simulations of charged NPs with the lipid membrane and prevented the unphysical freezing of water on the NP surface.[53] The lipid parameters were modified by the proposal of Wu *et al.* based on the original Martini force field.[54] In CGMD simulations, silicon was represented by the Q_0 bead and oxygen is represented by the Q_a bead. The CG polarizable silica NP consisted of a silicon bead and oxygen bead, where each silicon bead carried +2 charge and each oxygen bead carried −1 charge except for partial surface beads. 30% random surface silicon beads carried +3 charge for the positively charged NP and +1 charge for the negatively charged NP to make the surface charge close to the value measured by experiments.[32] The charge distribution of the surface beads in the CG polarizable silica NP was determined by an in-house Matlab® script that is provided in the ESI.† Note that the charge of silicon and oxygen beads can be also assigned using other protocols.[55,56] The bond parameters were followed by previous calibration that accorded with the CG degree of the Martini force field.[56]

Due to the limitation of current computing power, the diameter of NP was set 13 nm as large as we could to eliminate the size effect of the NP. To study the interaction of NPs with a LS bilayer, the NP was deposited above 1 nm of a pre-equilibrated LS bilayer (45 nm × 45 nm) under zero surface tension and the initial structure of the LS bilayer was generated using the insane.py package.[57] To study the interaction of NPs with dispersed LS molecules, NP and LS phospholipids were randomly set in a cube of 30 nm × 30 nm × 30 nm using the Packmol package[58] and solvated in a larger water box of 35 nm × 35 nm × 35 nm. Na and Cl ions were added in simulations for neutralizing the system charge if necessary.

Simulation details

Simulations were performed in NPT ensembles using the semi-isotropic Berendsen barostat to study the interactions of the NP with the LS bilayer and the isotropic Berendsen barostat to study the interactions of the NP with dispersed LS molecules. The pressure coupling constant was set as 2 ps and the system compressibility was set as 4.5×10^{-5} bar^{-1}. The time step was 20 fs and the neighbor list was updated every 10 steps. Temperature was maintained at 310 K by Berendsen temperature coupling with a coupling constant of 1.0 ps for NP and LS molecules according to the Martini force field,[51] and 0.2 ps for water and ions, as used by Wu *et al.*[53] Electrostatic interactions were calculated using the particle-mesh-Ewald method. All CGMD simulations were performed using the Gromacs 4.6.5 package.[59]

Results and discussion

Preparation for probing the lipid corona on the NPs from a natural LS

The silica NP is one of the most extensively studied materials for NP–lipid interactions due to its biocompatibility, hydrophilicity, and chemical stability, and is also one of the most accessible airborne NPs to the respiration system.[47,60–64] Considering that charge plays an important role in the interactions of NPs with the whole pulmonary system,[65,66] we hence investigated silica NPs with different surface charges, namely positively charged, neutral, and negatively charged based on their zeta potential. The characterization of the NPs, including transmission electron microscopy (TEM), dynamic light scattering (DLS) and zeta potential measurements, is shown in ESI† Table S1 and Fig. S1. Since the inhaled NPs can either translocate across the air–blood barrier within 1 hour or retain in the deep lung for 24 hours,[67,68] we incubated NPs with LS for 1 hour or 24 hours, respectively. In addition, the effect of sonication on interactions of NPs with LS was also examined, which has been traditionally used to promote the adsorption of liposome on NPs.[18,44,69] After incubation, the NP–LS complex was centrifuged through a sucrose cushion and directly recentrifuged followed by resuspension into a new tube to allow the rapid separation of unbound LS and avoid adsorption of LS on the tube surface during the centrifugation (Fig. 1A).[6]

Curosurf® was used as the LS model in this study. About 150 lipids were detected in the LS model by LC-MS analysis, and the detailed lipidomic data are listed in Table S2† determined by three independent biological repeats. The most abundant species in the LS was zwitterionic phosphatidylcholine (PC) that accounted for 69.9% of total lipids by mole ratio and the main constituent in the LS was dipalmitoylphosphatidylcholine (DPPC) (Fig. 1B and Table S2†). Zwitterionic sphingomyelin (SM) was the second most abundant species and comprised 20.2% of the total lipids. Note that the large proportion of SM

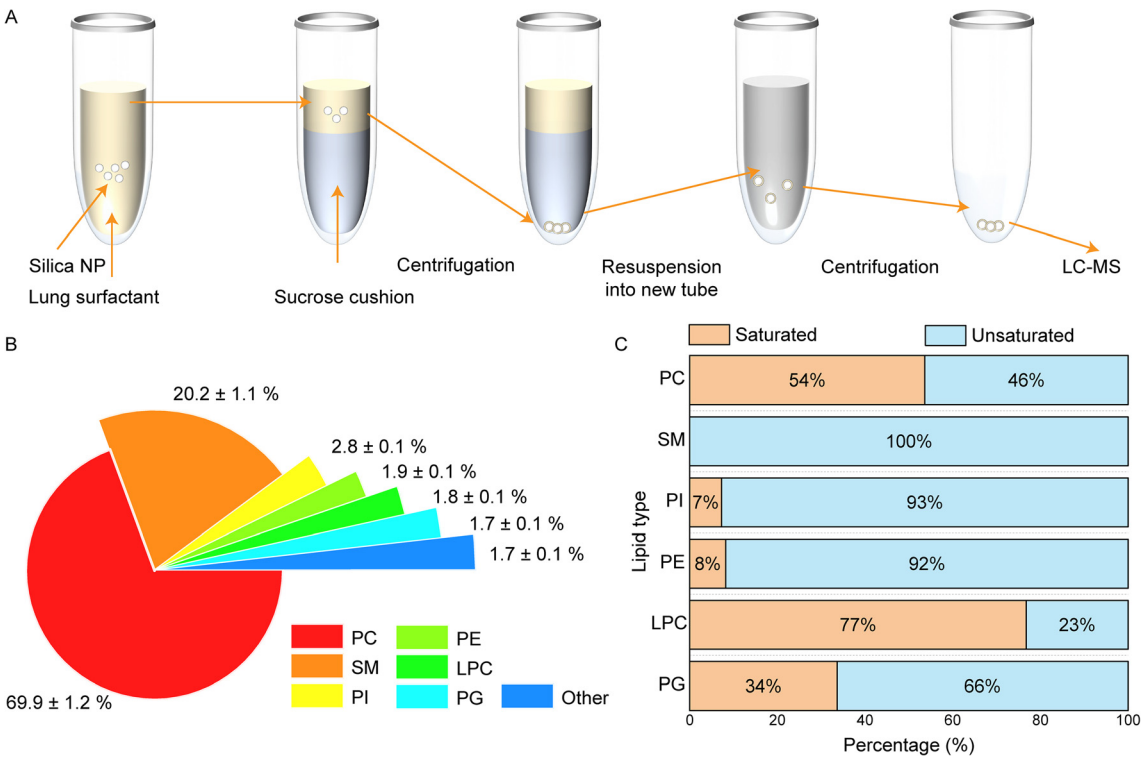

Fig. 1 Preparation for probing the lipid corona on the NPs from a natural LS. A. Illustration of the preparation and separation of the LP–LS corona complex. B and C. Classification of lipid components of the LS model (Curosurf®) based on lipid species and tail saturation as determined by LC-MS. Three independent biological repeats were performed to determine the lipidomics of the LS model.

in Curosurf® is due to the impurity of minced lung tissues.[31] PI (2.8%) and PG (1.7%) were the two main types of anionic phospholipids that led to a negative surface charge of the LS (Table S3†). Phosphatidylethanolamine (PE, 1.9%), lysophosphatidylcholine (LPC, 1.8%) and other types of lipids (1.7%), including phosphatidic acid (PA), phosphatidylserine (PS), lysophosphatidylinositol (LPI), and lysophosphatidylserine (LPS), were also detected by LC-MS. Among these phospholipids, the unsaturated phospholipids comprised about half of the total lipids, especially rich in the SM, PI, and PE (Fig. 1B). Since proteins and cholesterol make up a very low percentage in Curosurf®, they were not the subject of the present study. Overall, the lipid composition of the present LS model was close to human LS except for a higher proportion of SM and a lower proportion of PG and PE.[31,70]

Measurement of the lipid corona on NPs with different surface charges

The first issue is to determine whether the lipid corona is formed. The present LC-MS revealed that the amount of the adsorbed lipids was influenced both by surface charge and incubation conditions (Fig. 2). For comparison, we also listed our and other's results with corresponding conditions in Table 1. First, no obvious adsorption of the lipids (range from 0.0024 μmol to 0.0042 μmol) was found on the surface of negatively charged NPs regardless of incubation conditions compared with the control group (0.0016 μmol), demonstrating a strong repulsion of the negatively charged NPs with the LS. This finding agrees with others' measurements that used secondary ion mass spectrometry (SIMS) and job scattering plots to demonstrate a very weak adsorption of Curosurf® on bare silica NPs.[29,32] As shown by existing LC-MS measurements, the density of the adsorbed lipids on other negatively charged NPs, including polyethylene glycol (PEG) NP, carboxylic poly (lactic-*co*-glycolic-acid) (PLGA) NP, and Si–CeO_2 NP, ranges from 0.12–1.19 mg m^{-2},[17,71] which is also all far less than the one (4.01 mg m^{-2}) required to totally wrap the NPs with a bilayer (the detailed calculation is shown in Note S1 in the ESI†). Collectively, we can deduce that a complete lipid corona is hardly developed on the negatively charged NPs. Note that Mousseau *et al.* specially tuned the solution of bare silica NPs to pH 6.4, so that at least 43% NPs can be wrapped with a LS bilayer after 24-hour incubation in Curosurf® because of extra electrostatic attractions for NPs with the lipids.[34]

Although the neutral NPs did not adsorb much more lipids (0.0061 μmol) than the negatively charged NPs (0.0042 μmol) after 1-hour incubation, they can adsorb about three-fold more lipids (0.0181 μmol) through sonication (Fig. 2). Note that the lipid adsorption on the neutral NPs under 24-hour incubation was not presented here due to the inevitable aggregation of the neutral NPs in the solution. Considering the loss of lipids through the separation process and the lipids and proteins undetected by LC-MS, the density of the adsorbed lipids on the neutral NPs after sonication (2.83 mg m^{-2}) was close to 4.02 mg m^{-2} for a full wrap on the NP. Thus, we argue that the lipids adsorbed on most of these NPs should have already developed a complete lipid bilayer corona. We previously demonstrated that the hydrophobic surfactant proteins appear in a lipid bilayer corona on the hydrophilic NP by directly interacting with lipids rather than the NP itself, only slightly influencing the overall structure of the lipid corona at a protein concentration of 2% in wt%.[27] Therefore, we believe that the 1% hydrophobic surfactant proteins in Curosurf® were also present in the lipid corona, and their effects on the formation of the lipid corona should be insignificant.

The aminated silica NPs had a positive zeta-potential and spontaneously adsorbed abundant lipids (0.039 μmol) on their surface after 1 hour incubation (Fig. 2). Because integrated LS vesicles tend to directly adhere on positively charged NPs rather than wrap the NPs,[32,71] the density of the adsorbed lipids on the positively charged NPs under 1-hour incubation (5.83 mg m^{-2}) would be larger than that required to fully wrap the NP (4.02 mg m^{-2}). When sonication was applied or incubation time increased to 24 hours, the amount of adsorbed lipids on the positively charged NPs decreased instead, accompanied by the decrease of density to 2.79 mg m^{-2} and 3.10 mg m^{-2} that were close to the predicted value of 4.02 mg m^{-2}. Therefore, our results suggest that it needs long-time incubation or external force to facilitate the internalization of NPs by the lipid bilayer and thus develop a complete LS lipid corona on the positively charged NPs. Previous cryo-transmission electron microscopy (cryo-TEM) observations have also confirmed that at almost 80% of positively charged silica NPs were wrapped with a LS bilayer after 24-hour incubation with Curosurf® and this value increased to 100% when sonication was applied.[34]

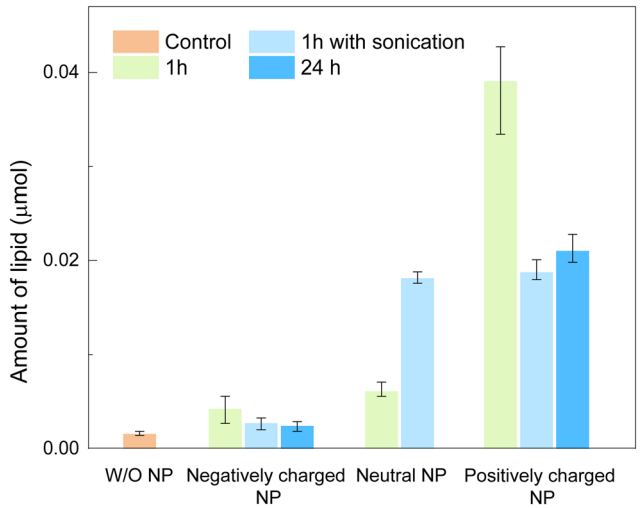

Fig. 2 Absolute amount of the lipids adsorbed on three types of silica NPs under 1-hour, 1-hour with sonication and 24-hour incubation at 37 °C as revealed by LC-MS. Data represents mean ± SD with positive and negative error bars (n = 3). Note that the lipid adsorption on the neutral NPs under 24-hour incubation was not presented here due to the inevitable aggregation of the neutral NPs in the solution.

Table 1 Experimental conditions, methods and measurements used to determine the lipids adsorbed on different types of NPs from LSs. The measurements from other groups are also listed for comparison

NP charge	NP type	LS model	Incubation condition	Separation method	Measurement method	Lipid density	Ref.
—	—	Curosurf® bilayer	Zero surface tension	—	MD simulation	4.02 mg m^{-2}	—
Negative	Unmodified silica	Curosurf®	1 h/24 h/sonication	Density centrifugation	LC-MS	Almost none	—
	Unmodified silica	Curosurf®	Continuous variation method	—	Job scattering plots	No interaction	32
	Unmodified silica	Curosurf®	Sonication	Centrifugation in D_2O	SIMS	Almost none	29
	Unmodified silica	Curosurf®	Sonication	Differential centrifugal sedimentation	Cryo-TEM	>43% NPs coated by supported bilayer	34
	PEG	BALF of pigs	1 h with shaking	Magnetic separation	LC-MS	0.12 mg m^{-2}	17
	Carboxylic PLGA	BALF of pigs	1 h with shaking	Magnetic separation	LC-MS	0.38 mg m^{-2}	17
	Si–CeO_2	BALF of rats	30 min	Centrifugation	LC-MS	1.19 mg m^{-2}	71
Neutral	Aminated silica	Curosurf®	Sonication	Density centrifugation	LC-MS	2.83 mg m^{-2}	—
Positive	Aminated silica	Curosurf®	1 h	Density centrifugation	LC-MS	5.83 mg m^{-2}	—
	Aminated silica	Curosurf®	Sonication/24 h	Density centrifugation	LC-MS	2.79/3.10 mg m^{-2}	—
	Aminated silica	Curosurf®	Continuous variation method	—	Job scattering plots	Form aggregation	32
	CeO_2	BALF of rats	30 min	Centrifugation	LC-MS/cryo-TEM	1.76 mg m^{-2}/multilayer adhesion	71
	Aminated silica	Curosurf®	24 h	Differential centrifugal sedimentation	Cryo-TEM	~80% NPs coated by supported bilayer	34
	Aminated silica	Curosurf®	Sonication	Differential centrifugal sedimentation	Cryo-TEM	Supported bilayer	18, 34

Comparison of the lipid composition in the corona and in the bulk LS

Since the types of lipids play a critical role in biological recognition,[70] it is necessary to identify the distribution of lipid species in coronas. Thus, we took advantage of LC-MS to examine the relative distribution of lipid species, including the major zwitterionic (PC, SM and PE) and anionic lipids (PI, PG, and PS), in coronas on positively charged (Fig. 3A) and neutral NPs (Fig. S2†). PC, as the most abundant lipid species in the lipid corona, exhibited a slight increase in proportion to about 80% by average of three conditions on positively charged NPs compared to 69.9% in the bulk LS (as shown in the absolute lipid distribution in Fig. S3†). In contrast, the ratio of SM significantly decreased in the lipid corona under all three conditions: 0.57 for 1-hour incubation, 0.42 for 1-hour incubation with sonication, and 0.39 for 24-hour incubation (Fig. 3A). Such a decrease in SM along with the increase in PC was also observed in the lipid corona on neutral NPs after sonication incubation (Fig. S2†). PE was also found to be depleted under all conditions on positively charged NPs. Since PC is more favorable in cellular uptake than SM and PE,[72,73] the increase of PC with the decrease of SM and PE in composition of the corona may be beneficial for the cellular uptake of the corona–NP complex. Although LS lipid coronas on other types of NPs show similar changes in their composition,[71] the amounts of the adsorbed lipids on these NPs are far less than those on the positively charged NPs, thus weakly affecting the biological recognitions.

Anionic lipids, including PI, PG and PS, in lipid coronas can provide pulmonary recognitions for NPs to enhance the clearance of NPs by pulmonary macrophages.[23,25] They were enriched in the coronas on the positively charged NPs after sonication or 24-hour incubation, possibly due to the strong electrostatic attractions between the lipids and NPs. Such an increase of the proportion of anionic lipids in the corona potentially promotes the clearance for the corona–NP complex by pulmonary macrophages. Meanwhile the enrichment of anionic lipids was not found in the corona on the neutral NPs after sonication incubation (Fig. S2†). It should be noted that the human LS has more abundant anionic lipids and thus may be more susceptible to the positively charged NPs than the present LS model.[70] After the lipid corona masks the surface of NPs, it also alters the surface properties of the NPs to influence their subsequent interactions with biological systems. For example, NPs become negatively charged and more hydrophobic with a complete LS corona coating,[27] where the negative surface charge enhances the translocation of the NPs through the lung[68] and mitigates the immune responses,[74] and the increase of hydrophobicity could promote the cellular uptake for NPs.[75]

The property of lipid tails, such as the saturation degree and length, is also an indispensable factor in the adsorption

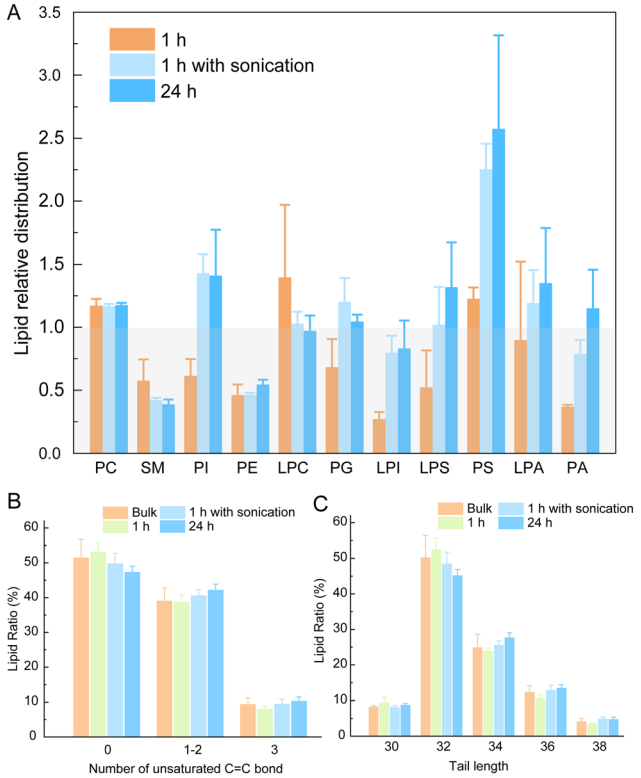

Fig. 3 The composition of the lipid corona on the positively charged NPs differs from that of the bulk LS. A. Relative lipid distribution in the corona on the positively charged NPs based on lipid species. Data represents mean ± SD (n = 3). The relative lipid distribution was defined as the ratio of the lipid proportion in the corona to that in the bulk LS. The values above and below unity indicated favorable and not favorable adsorption to NPs. The proportion of the lipid species in the corona is in the order from PC to PA. B and C. Absolute lipid proportion in the lipid corona based on the saturation degree and length of the tails. Data represents mean ± SD (n = 3). SM was not included in this analysis.

behavior and biophysical function of LS.[11] Unsaturated lipids are flexible and favorable to the high curvature, while saturated lipids are rigid and tend to arrange in a flat membrane.[76] Consistent with this fact, data in Fig. 3B show that unsaturated lipids bound to NPs more preferably than saturated lipids. Meanwhile, in the present LS model, the lipids with longer tails had a higher unsaturation degree (Fig. S4†) and thus tended to adsorb on the NPs rather than those with shorter tails (Fig. 3C). These results suggest that the positively charged NPs depleted more unsaturated lipids than saturated lipids in the LS by forming a lipid corona, which would lead to the local disturbance in the lipid distribution and mechanical properties of the LS membrane.

Effect of surface charge on the interactions between NPs and lipids

Although the above experiments have demonstrated the importance of the surface charge in the development of the lipid corona, how the surface charge influences the interactions of NPs with LS is still obscure due to the limited molecular details. We employed coarse-grained molecular dynamics (CGMD) simulations by the Martini force field[51] with a polarizable water and silica model[53,56] to inspect the molecular interactions between the anionic/cationic silica NPs and the LS bilayer (Fig. 4A). We set up the CGMD LS model directly based on the composition from the LC-MS measurements (Fig. 4B and Table S4†) instead of using a normal simplified LS model.[16,27] Because lipids in LS solutions tend to form vesicular structure with diameter over hundreds of nanometers (Table S3†),[17,18] we here used the lipid bilayer model to mimic the interactions of silica NPs and LS lipids. As a result, the anionic NP only weakly adhered on the bilayer, while the cationic NP caused a significant bilayer bending upon the NP attachment (Fig. 4C and D). Such a difference was caused by the five-fold higher interaction energy of the cationic NP with the LS than that of the anionic NP to assist the LS bilayer in the wrap of the NP by overcoming the bending energy (Fig. 4E). Note that the partial wrapping rather than total wrapping of the cationic NP is limited by the timescale in simulations, since the spontaneous wrapping of the NP by the lipid bilayer takes a long time to complete.[77] By contrast, when NPs interacted with the dispersed LS, both the anionic and cationic NPs could be encapsulated into a vesicular structure driven by the self-assembly (Fig. S5†), which was consistent with previous simulations.[27,28] In these cases, before the lipids came into contact with the NP, they formed micelle structures that were unstable due to the high curvature and thus favored to adsorb on the NP's surface to eliminate such a high curvature state. Therefore, the surface charge significantly influenced the interactions between NPs and lamellar LS, but had little effect on the interactions between NPs and dispersed LS. Combining the simulations and the LC-MS results (Fig. 2), we could conclude that continuous lamellar LS rather than dispersed LS directly adsorbed on the NPs upon the contact of NPs with LS.

Since electrostatic and van der Waals interactions play vital roles in the interactions between the NPs and lipids,[40,42] we explored how they influenced the interactions between the NPs and LS lipids in Fig. 4F. Zwitterionic lipids provided the major attractions with the NPs due to their overwhelming proportion in LS. Anionic lipids contributed moderate attractions with the cationic NP despite their low proportion in LS, but showed repulsion to the anionic NP. Surprisingly, by comparing the interaction energy per lipid (Fig. S6†), we found that the cationic NP not only interacted more strongly with an individual anionic lipid but also with a zwitterionic lipid than the anionic NP. This result accords with an existing measurement that validated a strong adsorption of zwitterionic PC on the cationic Au-NPs and no adsorption on the anionic Au-NPs.[78] These results suggested that the positive charge enhanced the attractions of NPs with both zwitterionic and anionic lipids, while the negative charge prevented the adsorption of the LS due to the electrostatic repulsion by anionic lipids.

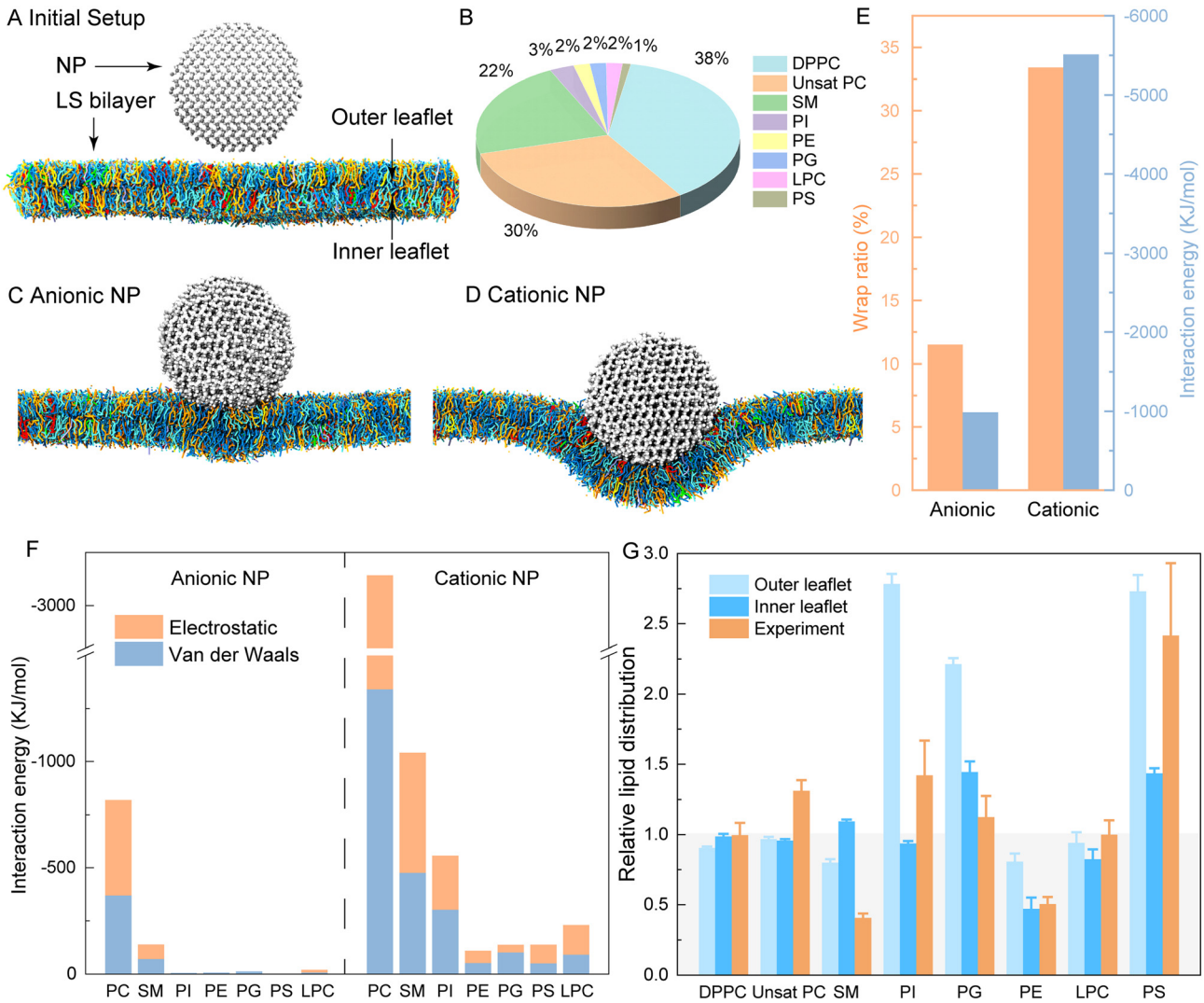

Fig. 4 Molecular view of the interactions between the LS and the anionic and cationic silica NPs. A. Initial setup for simulating the interactions of silica NPs with the LS bilayer in the section view. The NP and LS were all immersed into water, where water was not shown for clarity. B. Composition of the LS model used for simulations. C and D. Snapshots for the final structure of the interactions of the LS bilayer with the anionic NP and cationic NP in the section view. The system of the LS bilayer and NPs was considered to reach the equilibrium as the interaction energy did not significantly change (Fig. S7†). E. Interaction energy of the NPs with the LS bilayer and the wrap ratio obtained from the equilibrated structure. F. Electrostatic and van der Waals interaction energy of anionic and cationic NPs with the different lipid species in the LS bilayer. G. Relative lipid distribution in two leaflets around the cationic NP compared with the experimental data from1 h incubation with sonication and 24 h incubation. Data represents mean ± SD (n = 6).

With the ability to provide molecular details unavailable in experiments, the present CGMD simulations also revealed how the lipids were sorted by the cationic NP as shown in the lipid distribution in two leaflets wrapping the NPs (Fig. 4G). The distribution of PC was relatively stable in two leaflets except for a slight depletion of saturated DPPC in the outer leaflets. SM was obviously depleted in the outer leaflet because of its large stiffness, similar to the lipid sorting in a plasma membrane induced by curvature.[79] Anionic lipids, including PI, PG and PS, were significantly abundant in the outer leaflet, because they come into direct contact with the cationic NPs. The depletion of PE was pronounced in both two leaflets possibly due to its small head group that is disadvantageous for the curvature of the NP. Generally, when the LS bilayer wrapped the NP, strong attractions between the cationic NP and anionic lipids led to a significant enrichment of anionic lipids, and the intrinsic structure of SM and PE made them deplete. However, our simulations suggested that the enrichment of anionic lipids in the corona would slightly influence the biological recognitions of the NP–corona complex because they were not obviously enriched in the outer layer of the corona.

Conclusions

By mixing silica NPs with a natural LS, we find that surface charge of NPs is crucial to the development of the lipid corona as revealed by LC-MS. The negatively charged NPs

hardly adsorb lipids regardless of incubation conditions, whereas a complete lipid corona can be formed on neutral and positively charged NPs after 1-hour incubation with sonication, and on positively charged NPs after 24-hour incubation. In addition, the composition of the lipid corona formed on the positively NP differs from that of the bulk LS, with an increase in the proportion of PC and anionic lipids, but a decrease in the proportion of SM and PE. With the assistance of the molecular simulations, we demonstrate that the NPs interact with the lamellar LS bilayer rather than the dispersed LS. In this model, electrostatic interactions provide repulsion between the anionic lipids and the negatively charged NP to prevent their further interactions, while providing extra interaction strength for the positively charged NP with both zwitterionic and anionic lipids to promote the wrap of the NP by a LS bilayer. Besides, the simulations reveal that the difference in the composition between the adsorbed lipids and bulk LS is caused by the affinity of the NP with the lipid and the intrinsic structure of the lipid.

Author contributions

Xuan Bai: conceptualization, methodology, investigation, formal analysis, visualization, funding acquisition, writing – original draft. Sin Man Lam: methodology, investigation. Pengcheng Nie: investigation. Ming Xu: methodology, supervision, resources. Sijin Liu: supervision, resources. Guanghou Shui: conceptualization, supervision, resources, funding acquisition. Guoqing Hu: conceptualization, supervision, project administration, formal analysis, resources, funding acquisition, writing – review & editing. Xuan Bai and Sin Man Lam contributed equally to this work.

Conflicts of interest

There are no conflicts to declare.

Acknowledgements

This work was supported financially by the National Natural Science Foundation of China (11832017), the Chinese Academy of Sciences Strategic Priority Research Program (XDB22040403), the National Key R&D Program of China (2018YFA0800901, 2018YFA0506900), and the China National Postdoctoral Program for Innovative Talents (BX20200298). The MD simulations were performed on TianHe-2 at the National Supercomputing Center in Guangzhou.

References

1 C. Y. Zhang, L. Yan, X. Wang, S. Zhu, C. Y. Chen, Z. J. Gu and Y. L. Zhao, Progress, challenges, and future of nanomedicine, *Nano Today*, 2020, **35**, 101008.
2 Y. Hu, S. Mignani, J. P. Majoral, M. Shen and X. Shi, Construction of iron oxide nanoparticle-based hybrid platforms for tumor imaging and therapy, *Chem. Soc. Rev.*, 2018, **47**, 1874–1900.
3 S. Kusumoputro, S. Tseng, J. Tse, C. Au, C. Lau, X. Wang and T. Xia, Potential nanoparticle applications for prevention, diagnosis, and treatment of COVID-19, *View*, 2020, **1**, 20200105.
4 M. Hadjidemetriou and K. Kostarelos, Nanomedicine: Evolution of the nanoparticle corona, *Nat. Nanotechnol.*, 2017, **12**, 288–290.
5 M. P. Monopoli, C. Aberg, A. Salvati and K. A. Dawson, Biomolecular coronas provide the biological identity of nanosized materials, *Nat. Nanotechnol.*, 2012, **7**, 779–786.
6 S. Tenzer, D. Docter, J. Kuharev, A. Musyanovych, V. Fetz, R. Hecht, F. Schlenk, D. Fischer, K. Kiouptsi, C. Reinhardt, K. Landfester, H. Schild, M. Maskos, S. K. Knauer and R. H. Stauber, Rapid formation of plasma protein corona critically affects nanoparticle pathophysiology, *Nat. Nanotechnol.*, 2013, **8**, 772–781.
7 E. Casals, T. Pfaller, A. Duschl, G. J. Oostingh and V. Puntes, Time evolution of the nanoparticle protein corona, *ACS Nano*, 2010, **4**, 3623–3632.
8 M. Lundqvist, J. Stigler, T. Cedervall, T. Berggard, M. B. Flanagan, I. Lynch, G. Elia and K. Dawson, The Evolution of the Protein Corona around Nanoparticles: A Test Study, *ACS Nano*, 2011, **5**, 7503–7509.
9 P. C. Ke, S. Lin, W. J. Parak, T. P. Davis and F. Caruso, A Decade of the Protein Corona, *ACS Nano*, 2017, **11**, 11773–11776.
10 M. P. Monopoli, D. Walczyk, A. Campbell, G. Elia, I. Lynch, F. B. Bombelli and K. A. Dawson, Physical-chemical aspects of protein corona: relevance to in vitro and in vivo biological impacts of nanoparticles, *J. Am. Chem. Soc.*, 2011, **133**, 2525–2534.
11 Y. Y. Zuo, R. A. Veldhuizen, A. W. Neumann, N. O. Petersen and F. Possmayer, Current perspectives in pulmonary surfactant–inhibition, enhancement and evaluation, *Biochim. Biophys. Acta, Biomembr.*, 2008, **1778**, 1947–1977.
12 S. Rugonyi, S. C. Biswas and S. B. Hall, The biophysical function of pulmonary surfactant, *Respir. Physiol. Neurobiol.*, 2008, **163**, 244–255.
13 A. Hidalgo, A. Cruz and J. Perez-Gil, Pulmonary surfactant and nanocarriers: Toxicity versus combined nanomedical applications, *Biochim. Biophys. Acta, Biomembr.*, 2017, **1859**, 1740–1748.
14 X. B. Lin, T. T. Bai, Y. Y. Zuo and N. Gu, Promote potential applications of nanoparticles as respiratory drug carrier: insights from molecular dynamics simulations, *Nanoscale*, 2014, **6**, 2759–2767.
15 A. Rabajczyk, M. Zielecka, R. Porowski and P. K. Hopke, Metal nanoparticles in the air: state of the art and future perspectives, *Environ. Sci.: Nano*, 2020, **7**, 3233–3254.
16 G. Hu, B. Jiao, X. Shi, R. P. Valle, Q. Fan and Y. Y. Zuo, Physicochemical properties of nanoparticles regulate translocation across pulmonary surfactant monolayer and formation of lipoprotein corona, *ACS Nano*, 2013, **7**, 10525–10533.
17 S. S. Raesch, S. Tenzer, W. Storck, A. Rurainski, D. Selzer, C. A. Ruge, J. Perez-Gil, U. F. Schaefer and C. M. Lehr,

Proteomic and Lipidomic Analysis of Nanoparticle Corona upon Contact with Lung Surfactant Reveals Differences in Protein, but Not Lipid Composition, *ACS Nano*, 2015, **9**, 11872–11885.

18 F. Mousseau, C. Puisney, S. Mornet, R. Le Borgne, A. Vacher, M. Airiau, A. Baeza-Squiban and J. F. Berret, Supported pulmonary surfactant bilayers on silica nanoparticles: formulation, stability and impact on lung epithelial cells, *Nanoscale*, 2017, **9**, 14967–14978.

19 A. J. Chetwynd and I. Lynch, The rise of the nanomaterial metabolite corona, and emergence of the complete corona, *Environ. Sci.: Nano*, 2020, **7**, 1041–1060.

20 L. De Backer, K. Braeckmans, M. C. Stuart, J. Demeester, S. C. De Smedt and K. Raemdonck, Bio-inspired pulmonary surfactant-modified nanogels: A promising siRNA delivery system, *J. Controlled Release*, 2015, **206**, 177–186.

21 S. Vranic, I. Garcia-Verdugo, C. Darnis, J. M. Sallenave, N. Boggetto, F. Marano, S. Boland and A. Baeza-Squiban, Internalization of SiO(2) nanoparticles by alveolar macrophages and lung epithelial cells and its modulation by the lung surfactant substitute Curosurf, *Environ. Sci. Pollut. Res.*, 2013, **20**, 2761–2770.

22 M. Gasser, P. Wick, M. J. Clift, F. Blank, L. Diener, B. Yan, P. Gehr, H. F. Krug and B. Rothen-Rutishauser, Pulmonary surfactant coating of multi-walled carbon nanotubes (MWCNTs) influences their oxidative and pro-inflammatory potential in vitro, *Part. Fibre Toxicol.*, 2012, **9**, 17.

23 A. A. Kapralov, W. H. Feng, A. A. Amoscato, N. Yanamala, K. Balasubramanian, D. E. Winnica, E. R. Kisin, G. P. Kotchey, P. Gou, L. J. Sparvero, P. Ray, R. K. Mallampalli, J. Klein-Seetharaman, B. Fadeel, A. Star, A. A. Shvedova and V. E. Kagan, Adsorption of surfactant lipids by single-walled carbon nanotubes in mouse lung upon pharyngeal aspiration, *ACS Nano*, 2012, **6**, 4147–4156.

24 L. Zhang, J. Sun, Y. Wang, J. Wang, X. Shi and G. Hu, Nonspecific Organelle-Targeting Strategy with Core-Shell Nanoparticles of Varied Lipid Components/Ratios, *Anal. Chem.*, 2016, **88**, 7344–7351.

25 Y. Ogasawara, Y. Kuroki and T. Akino, Pulmonary surfactant protein D specifically binds to phosphatidylinositol, *J. Biol. Chem.*, 1992, **267**, 21244–21249.

26 C. A. Ruge, U. F. Schaefer, J. Herrmann, J. Kirch, O. Canadas, M. Echaide, J. Pérez-Gil, C. Casals, R. Müller and C.-M. Lehr, The interplay of lung surfactant proteins and lipids assimilates the macrophage clearance of nanoparticles, *PLoS One*, 2012, **7**, e40775.

27 Q. Hu, X. Bai, G. Hu and Y. Y. Zuo, Unveiling the Molecular Structure of Pulmonary Surfactant Corona on Nanoparticles, *ACS Nano*, 2017, **11**, 6832–6842.

28 H. Jing, Y. Wang, P. R. Desai, K. S. Ramamurthi and S. Das, Formation and Properties of a Self-Assembled Nanoparticle-Supported Lipid Bilayer Probed through Molecular Dynamics Simulations, *Langmuir*, 2020, **36**, 5524–5533.

29 W. Wohlleben, M. D. Driessen, S. Raesch, U. F. Schaefer, C. Schulze, B. Vacano, A. Vennemann, M. Wiemann, C. A. Ruge, H. Platsch, S. Mues, R. Ossig, J. M. Tomm, J. Schnekenburger, T. A. Kuhlbusch, A. Luch, C. M. Lehr and A. Haase, Influence of agglomeration and specific lung lining lipid/protein interaction on short-term inhalation toxicity, *Nanotoxicology*, 2016, **10**, 970–980.

30 H. Whitwell, R. M. Mackay, C. Elgy, C. Morgan, M. Griffiths, H. Clark, P. Skipp and J. Madsen, Nanoparticles in the lung and their protein corona: the few proteins that count, *Nanotoxicology*, 2016, **10**, 1385–1394.

31 O. Blanco and J. Perez-Gil, Biochemical and pharmacological differences between preparations of exogenous natural surfactant used to treat Respiratory Distress Syndrome: role of the different components in an efficient pulmonary surfactant, *Eur. J. Pharmacol.*, 2007, **568**, 1–15.

32 F. Mousseau and J. F. Berret, The role of surface charge in the interaction of nanoparticles with model pulmonary surfactants, *Soft Matter*, 2018, **14**, 5764–5774.

33 F. Mousseau, R. Le Borgne, E. Seyrek and J. F. Berret, Biophysicochemical Interaction of a Clinical Pulmonary Surfactant with Nanoalumina, *Langmuir*, 2015, **31**, 7346–7354.

34 F. Mousseau, E. K. Oikonomou, A. Vacher, M. Airiau, S. Mornet and J.-F. Berret, Revealing the pulmonary surfactant corona on silica nanoparticles by cryo-transmission electron microscopy, *Nanoscale Adv.*, 2020, **2**, 642–647.

35 S. Mornet, O. Lambert, E. Duguet and A. Brisson, The formation of supported lipid bilayers on silica nanoparticles revealed by cryoelectron microscopy, *Nano Lett.*, 2005, **5**, 281–285.

36 G. Gopalakrishnan, I. Rouiller, D. R. Colman and R. B. Lennox, Supported bilayers formed from different phospholipids on spherical silica substrates, *Langmuir*, 2009, **25**, 5455–5458.

37 J. W. Liu, A. Stace-Naughton, X. M. Jiang and C. J. Brinker, Porous Nanoparticle Supported Lipid Bilayers (Protocells) as Delivery Vehicles, *J. Am. Chem. Soc.*, 2009, **131**, 1354–1355.

38 H. Meng, M. Y. Wang, H. Y. Liu, X. S. Liu, A. Situ, B. Wu, Z. X. Ji, C. H. Chang and A. E. Nel, Use of a Lipid-Coated Mesoporous Silica Nanoparticle Platform for Synergistic Gemcitabine and Paclitaxel Delivery to Human Pancreatic Cancer in Mice, *ACS Nano*, 2015, **9**, 3540–3557.

39 U. Seifert, Configurations of fluid membranes and vesicles, *Adv. Phys.*, 1997, **46**, 13–137.

40 R. P. Richter, R. Berat and A. R. Brisson, Formation of solid-supported lipid bilayers: an integrated view, *Langmuir*, 2006, **22**, 3497–3505.

41 J. Liu, X. Jiang, C. Ashley and C. J. Brinker, Electrostatically mediated liposome fusion and lipid exchange with a nanoparticle-supported bilayer for control of surface charge, drug containment, and delivery, *J. Am. Chem. Soc.*, 2009, **131**, 7567–7569.

42 T. H. Anderson, Y. Min, K. L. Weirich, H. Zeng, D. Fygenson and J. N. Israelachvili, Formation of supported bilayers on silica substrates, *Langmuir*, 2009, **25**, 6997–7005.

43 S. Savarala, S. Ahmed, M. A. Ilies and S. L. Wunder, Formation and colloidal stability of DMPC supported lipid bilayers on SiO2 nanobeads, *Langmuir*, 2010, **26**, 12081–12088.

44 A. L. Troutier and C. Ladaviere, An overview of lipid membrane supported by colloidal particles, *Adv. Colloid Interface Sci.*, 2007, **133**, 1–21.
45 J. J. Liu, N. Y. Lu, J. L. Li, Y. Y. Weng, B. Yuan, K. Yang and Y. Q. Ma, Influence of Surface Chemistry on Particle Internalization into Giant Unilamellar Vesicles, *Langmuir*, 2013, **29**, 8039–8045.
46 C. A. Keller and B. Kasemo, Surface Specific Kinetics of Lipid Vesicle Adsorption Measured with a Quartz Crystal Microbalance, *Biophys. J.*, 1998, **75**, 1397–1402.
47 J. Liu, Interfacing Zwitterionic Liposomes with Inorganic Nanomaterials: Surface Forces, Membrane Integrity, and Applications, *Langmuir*, 2016, **32**, 4393–4404.
48 W. Zhang, A. J. Chetwynd, J. A. Thorn, I. Lynch and R. Ramautar, Understanding the Significance of Sample Preparation in Studies of the Nanoparticle Metabolite Corona, *ACS Meas. Sci. Au*, 2022, **2**, 251–260.
49 J. Y. Lee, H. Wang, G. Pyrgiotakis, G. M. DeLoid, Z. Zhang, J. Beltran-Huarac, P. Demokritou and W. Zhong, Analysis of lipid adsorption on nanoparticles by nanoflow liquid chromatography-tandem mass spectrometry, *Anal. Bioanal. Chem.*, 2018, **410**, 6155–6164.
50 S. M. Lam, C. Zhang, Z. Wang, Z. Ni, S. Zhang, S. Yang, X. Huang, L. Mo, J. Li, B. Lee, M. Mei, L. Huang, M. Shi, Z. Xu, F. P. Meng, W. J. Cao, M. J. Zhou, L. Shi, G. H. Chua, B. Li, J. Cao, J. Wang, S. Bao, Y. Wang, J. W. Song, F. Zhang, F. S. Wang and G. Shui, A multi-omics investigation of the composition and function of extracellular vesicles along the temporal trajectory of COVID-19, *Nat. Metab.*, 2021, **3**, 909–922.
51 S. J. Marrink, H. J. Risselada, S. Yefimov, D. P. Tieleman and A. H. de Vries, The MARTINI force field: Coarse grained model for biomolecular simulations, *J. Phys. Chem. B*, 2007, **111**, 7812–7824.
52 H. I. Ingolfsson, C. A. Lopez, J. J. Uusitalo, D. H. de Jong, S. M. Gopal, X. Periole and S. J. Marrink, The power of coarse graining in biomolecular simulations, *Wiley Interdiscip. Rev.: Comput. Mol. Sci.*, 2014, **4**, 225–248.
53 Z. Wu, Q. Cui and A. Yethiraj, A new coarse-grained model for water: the importance of electrostatic interactions, *J. Phys. Chem. B*, 2010, **114**, 10524–10529.
54 Z. Wu, Q. Cui and A. Yethiraj, A New Coarse-Grained Force Field for Membrane-Peptide Simulations, *J. Chem. Theory Comput.*, 2011, **7**, 3793–3802.
55 K. Kubiak and P. A. Mulheran, Molecular Dynamics Simulations of Hen Egg White Lysozyme Adsorption at a Charged Solid Surface, *J. Phys. Chem. B*, 2009, **113**, 12189–12200.
56 G. B. Yu and J. Zhou, Understanding the curvature effect of silica nanoparticles on lysozyme adsorption orientation and conformation: a mesoscopic coarse-grained simulation study, *Phys. Chem. Chem. Phys.*, 2016, **18**, 23500–23507.
57 T. A. Wassenaar, H. I. Ingolfsson, R. A. Bockmann, D. P. Tieleman and S. J. Marrink, Computational Lipidomics with insane: A Versatile Tool for Generating Custom Membranes for Molecular Simulations, *J. Chem. Theory Comput.*, 2015, **11**, 2144–2155.
58 L. Martinez, R. Andrade, E. G. Birgin and J. M. Martinez, PACKMOL: A Package for Building Initial Configurations for Molecular Dynamics Simulations, *J. Comput. Chem.*, 2009, **30**, 2157–2164.
59 B. Hess, C. Kutzner, D. van der Spoel and E. Lindahl, GROMACS 4: Algorithms for highly efficient, load-balanced, and scalable molecular simulation, *J. Chem. Theory Comput.*, 2008, **4**, 435–447.
60 R. Merget, T. Bauer, H. U. Kupper, S. Philippou, H. D. Bauer, R. Breitstadt and T. Bruening, Health hazards due to the inhalation of amorphous silica, *Arch. Toxicol.*, 2002, **75**, 625–634.
61 C. Brandenberger, N. L. Rowley, D. N. Jackson-Humbles, Q. Zhang, L. A. Bramble, R. P. Lewandowski, J. G. Wagner, W. Chen, B. L. Kaplan, N. E. Kaminski, G. L. Baker, R. M. Worden and J. R. Harkema, Engineered silica nanoparticles act as adjuvants to enhance allergic airway disease in mice, *Part. Fibre Toxicol.*, 2013, **10**, 26.
62 G. Oberdörster, A. Maynard, K. Donaldson, V. Castranova, J. Fitzpatrick, K. Ausman, J. Carter, B. Karn, W. Kreyling, D. Lai, S. Olin, N. Monteiro-Riviere, D. Warheit, H. Yang and A. r. f. t. I. R. F. R. S. I. N. T. S. W. Group, Principles for characterizing the potential human health effects from exposure to nanomaterials: elements of a screening strategy, *Part. Fibre Toxicol.*, 2005, **2**, 8.
63 C. Guo, Y. Liu and Y. Li, Adverse effects of amorphous silica nanoparticles: Focus on human cardiovascular health, *J. Hazard. Mater.*, 2021, **406**, 124626.
64 C. M. Sayes, K. L. Reed, K. P. Glover, K. A. Swain, M. L. Ostraat, E. M. Donner and D. B. Warheit, Changing the dose metric for inhalation toxicity studies: Short-term study in rats with engineered aerosolized amorphous silica nanoparticles, *Inhalation Toxicol.*, 2010, **22**, 348–354.
65 C. A. Fromen, T. B. Rahhal, G. R. Robbins, M. P. Kai, T. W. Shen, J. C. Luft and J. M. DeSimone, Nanoparticle surface charge impacts distribution, uptake and lymph node trafficking by pulmonary antigen-presenting cells, *Nanomedicine*, 2016, **12**, 677–687.
66 D. Q. Arick, Y. H. Choi, H. C. Kim and Y. Y. Won, Effects of nanoparticles on the mechanical functioning of the lung, *Adv. Colloid Interface Sci.*, 2015, **225**, 218–228.
67 W. Moller, K. Felten, K. Sommerer, G. Scheuch, G. Meyer, P. Meyer, K. Haussinger and W. G. Kreyling, Deposition, retention, and translocation of ultrafine particles from the central airways and lung periphery, *Am. J. Respir. Crit. Care Med.*, 2008, **177**, 426–432.
68 H. S. Choi, Y. Ashitate, J. H. Lee, S. H. Kim, A. Matsui, N. Insin, M. G. Bawendi, M. Semmler-Behnke, J. V. Frangioni and A. Tsuda, Rapid translocation of nanoparticles from the lung airspaces to the body, *Nat. Biotechnol.*, 2010, **28**, 1300–1303.
69 P. N. Durfee, Y. S. Lin, D. R. Dunphy, A. J. Muniz, K. S. Butler, K. R. Humphrey, A. J. Lokke, J. O. Agola, S. S. Chou, I. M. Chen, W. Wharton, J. L. Townson, C. L. Willman and C. J. Brinker, Mesoporous Silica Nanoparticle-Supported Lipid Bilayers (Protocells) for Active Targeting and Delivery to Individual Leukemia Cells, *ACS Nano*, 2016, **10**, 8325–8345.

70 R. Veldhuizen, K. Nag, S. Orgeig and F. Possmayer, The role of lipids in pulmonary surfactant, *Biochim. Biophys. Acta, Mol. Basis Dis.*, 1998, **1408**, 90–108.

71 N. V. Konduru, F. Damiani, S. Stoilova-McPhie, J. S. Tresback, G. Pyrgiotakis, T. C. Donaghey, P. Demokritou, J. D. Brain and R. M. Molina, Nanoparticle Wettability Influences Nanoparticle-Phospholipid Interactions, *Langmuir*, 2018, **34**, 6454–6461.

72 T. M. Allen, G. A. Austin, A. Chonn, L. Lin and K. C. Lee, Uptake of liposomes by cultured mouse bone marrow macrophages: influence of liposome composition and size, *Biochim. Biophys. Acta*, 1991, **1061**, 56–64.

73 K. D. Lee, K. Hong and D. Papahadjopoulos, Recognition of liposomes by cells: in vitro binding and endocytosis mediated by specific lipid headgroups and surface charge density, *Biochim. Biophys. Acta, Biomembr.*, 1992, **1103**, 185–197.

74 F. Blank, K. Fytianos, E. Seydoux, L. Rodriguez-Lorenzo, A. Petri-Fink, C. von Garnier and B. Rothen-Rutishauser, Interaction of biomedical nanoparticles with the pulmonary immune system, *J. Nanobiotechnol.*, 2017, **15**, 6.

75 X. Bai, S. Q. Wang, X. L. Yan, H. Y. Zhou, J. H. Zhan, S. J. Liu, V. K. Sharma, G. B. Jiang, H. Zhu and B. Yan, Regulation of Cell Uptake and Cytotoxicity by Nanoparticle Core under the Controlled Shape, Size, and Surface Chemistries, *ACS Nano*, 2020, **14**, 289–302.

76 H. J. Risselada and S. J. Marrink, Curvature effects on lipid packing and dynamics in liposomes revealed by coarse grained molecular dynamics simulations, *Phys. Chem. Chem. Phys.*, 2009, **11**, 2056–2067.

77 R. Michel, E. Kesselman, T. Plostica, D. Danino and M. Gradzielski, Internalization of Silica Nanoparticles into Fluid Liposomes: Formation of Interesting Hybrid Colloids, *Angew. Chem., Int. Ed.*, 2014, **53**, 12441–12445.

78 X. Zhang, A. K. Pandiakumar, R. J. Hamers and C. J. Murphy, Quantification of Lipid Corona Formation on Colloidal Nanoparticles from Lipid Vesicles, *Anal. Chem.*, 2018, **90**, 14387–14394.

79 S. Baoukina, H. I. Ingolfsson, S. Marrink and D. P. Tieleman, Curvature-Induced Sorting of Lipids in Plasma Membrane Tethers, *Adv. Theory Simul.*, 2018, **1**, 1800034.